JACS Au
AN OPEN ACCESS JOURNAL OF THE AMERICAN CHEMICAL SOCIETY

pubs.acs.org/jacsau
Article

Sluggish Electron Transfer of Oxygen-Terminated Moderately Boron-Doped Diamond Electrode Induced by Large Interfacial Capacitance between a Diamond and Silicon Interface

Atsushi Otake, Taiki Nishida, Shinya Ohmagari, and Yasuaki Einaga*

Cite This: JACS Au 2024, 4, 1184−1193
Read Online

ABSTRACT: Boron-doped diamond (BDD) has tremendous potential for use as an electrode material with outstanding characteristics. The substrate material of BDD can affect the electrochemical properties of BDD electrodes due to the different junction structures of BDD and the substrate materials. However, the BDD/substrate interfacial properties have not been clarified. In this study, the electrochemical behavior of BDD electrodes with different boron-doping levels (0.1% and 1.0% B/C ratios) synthesized on Si, W, Nb, and Mo substrates was investigated. Potential band diagrams of the BDD/substrate interface were proposed to explain different junction structures and electrochemical behaviors. Oxygen-terminated BDD with moderate boron-doping levels exhibited sluggish electron transfer induced by the large capacitance generated at the BDD/Si interface. These findings provide a fundamental understanding of diamond electrochemistry and insight into the selection of suitable substrate materials for practical applications of BDD electrodes.

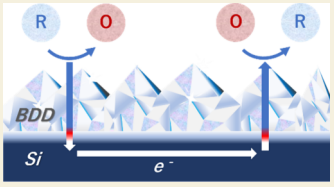

KEYWORDS: *boron-doped diamond, substrate materials, interfacial capacitance, electrode, electrochemistry*

1. INTRODUCTION

Diamond exhibits the highest hardness among known materials, the highest thermal conductivity at room temperature, high transparency over a wide range of wavelengths, and remarkable physical and chemical stability in harsh environments. Diamond is a highly resistive material with a bandgap of 5.47 eV and shows resistance values on the order of 10^{16} Ω·cm. It can be an electrically conductive material by surface termination or impurity doping. Hence, conductive diamond has tremendous potential as a material for electronics[1−5] and electrode[6−9] materials.

Landstrass et al. reported that the surface of diamond synthesized by chemical vapor deposition (CVD) exhibits electrical conductivity.[10] This conductivity is attributed to the p-type conductivity of the hydrogen- (H-) terminated diamond surface, which acts as acceptor like surface energy states,[11] owing to the surface dipole moment generated by the electronegativities of C (2.5) and H (2.1) atoms.[12−14] These conductive surfaces of H-terminated diamonds can be used in the construction of semiconductor devices such as p-n and Schottky diodes as well as field effect transistors (FETs), which have attracted significant attention especially in power semiconductor devices due to their extremely high career mobility and electric breakdown field.[15,16]

Another approach for conductive diamond is impurity doping. Phosphorus-doping affords n-type semiconductor diamonds,[17−20] and boron-doping affords p-type semiconductor diamonds.[21−23] In particular, boron-doped diamond (BDD) could serve as a next-generation electrode material owing to its large potential window, small background current, superior biocompatibility, and surface functionalization capability.[24−27]

Conductive diamond is mainly synthesized by CVD.[28] In particular, single-crystalline CVD diamonds are synthesized via homoepitaxial growth on a single crystalline diamond substrate[29,30] or heteroepitaxial growth on nondiamond substrates.[31−34] These CVD single-crystalline diamonds have broad applications in devices,[35−37] and attempts to understand their conductive mechanism are in progress.[38−43] However, single-crystalline diamond has drawbacks such as significant cost and difficulties due to the large size of single-crystalline diamond substrates and limitation of the substrate materials for heteroepitaxial diamond growth, hindering its practical application as an electrode material.

In contrast, polycrystalline diamond as an electrode material demonstrates a rapid CVD growth rate as well as high carrier concentrations and tunable conductivity by controlling the boron-doping levels. Moreover, large-size substrates are available for industrial applications.[44−47] Polycrystalline diamonds are typically synthesized on substrates like single-crystalline Si substrates or metal substrates such as W, Nb, Mo, Ta, and Ti.[6,48,49] The conductive mechanism of polycrystalline

Received: January 3, 2024
Revised: February 10, 2024
Accepted: February 26, 2024
Published: March 8, 2024

diamonds has been studied in terms of surface termination and boron-doping levels,[50−58] but reports on the effects of the substrate material are limited.[59] In particular, the interfacial properties between a BDD and its substrate have not yet been investigated.

BDD acts as a p-type extrinsic semiconductor, because C atoms are replaced by B atoms with fewer valence electrons, thus making it an electron acceptor. Notably, metal−semiconductor junctions are formed at the BDD/metal substrate interface, whereas semiconductor heterojunctions are formed at the BDD/Si substrate interface. In metal−semiconductor junctions, Schottky barriers are possibly formed. In semiconductor heterojunctions, energy barriers called band discontinuities are possibly formed. In both cases, the interfacial energy barriers are normally accompanied by interfacial capacitances,[60−63] which consequently influence the electron transfer at the BDD−substrate interface and the electrochemical properties of BDD electrodes. Therefore, selecting a suitable substrate material and understanding the electron-transfer mechanism at the interface are crucial.

In this study, we investigated the effects of the substrate material on the electrochemical properties of the BDD electrodes. Different BDD electrodes were synthesized with different amounts of boron-doping on Si and metal substrates (W, Nb, and Mo), and their electrochemical properties were characterized. Subsequently, theoretical studies were conducted on the electron transfer at the BDD/substrate interface as well as at the BDD/electrolyte interface, and band diagrams were proposed to explain their effects on the electrochemical behavior of the BDDs. Then, the electrical properties of BDD were experimentally investigated to validate the proposed band diagrams.

2. EXPERIMENTAL SECTION

2.1. Materials

Sulfuric acid (H_2SO_4), nitric acid (HNO_3), potassium chloride (KCl), potassium ferrocyanide ($K_4[Fe(CN)_6]$), methanol, and acetone were purchased from Wako Pure Chemical Industries, Ltd. and hexaammineruthenium(III) chloride ($[Ru(NH_3)_6]Cl_3$) was purchased from Sigma-Aldrich. These materials were used without purification. Deionized (DI) water was obtained from a water purification system (Milli-Q Reference A+, MERCK Millipore) with a resistivity of 18.2 MΩ·cm at 25 °C. The experiments were performed at room temperature (25 °C) under atmospheric pressure, unless otherwise stated.

2.2. Synthesis of the BDD Films Using Si and Metal Substrates and Characterization of BDD Film Surfaces

Two-inch p-type Si wafers with a (100) orientation, resistivity of 0.005−0.01 Ω·cm, and thickness of 0.75 mm were used as substrates. The carrier concentrations of the p-Si wafer were estimated using a resistivity of ∼1.0 × 10^{19} cm^{-3} from the Irvin curve.[64] High-purity metal sheets (W: 99.95%, Nb: 99.9%, and Mo: 99.95%) with a 1.0 mm thickness and 50 mm diameter were used, as well as ceramic plates made from aluminum oxide (ALO) with a 1.0 mm thickness and 10 mm square size. Before BDD deposition, the Si substrate was abraded with microdiamond powder (∼1 μm), while the metal and ALO substrates were polished with #320 sandpaper and then cleaned by ultrasonication with methanol. The substrates were seeded via ultrasonication in a diluted nanodiamond suspension for 30 min (NanoAmando, NanoCarbon Research Institute Limited, Japan). BDD thin films were grown on Si(100) and W, Nb, and Mo substrates using a microwave plasma-assisted chemical vapor deposition system (MWPCVD, AX6500X, CORNES Technologies Corp.) as described previously.[55] The boron source, trimethylboron ($B(CH_3)_3$), and the carbon source, methane (CH_4), were supplied into the hydrogen plasma at B/C atomic ratios of 0.1% and 1.0%. The deposition time was 6 h.

The surfaces of the as-prepared BDD films were characterized by using a Raman spectrometer (Acton SP2500, Princeton Instruments) with an excitation wavelength of 532 nm and a benchtop scanning electron microscope (SEM, JCM-6000Plus, JEOL Ltd.). The Raman spectra and SEM images of BDDs are shown in Figures S9 and S10.

2.3. Surface Termination and Electrochemical Measurements of BDD Electrodes

A single-compartment, three-electrode PTFE cell was used for the electrochemical measurements. A BDD electrodes, a Pt plate, and Ag/AgCl (saturated KCl) were equipped as the working, counter, and reference electrodes, respectively. An electrochemical station, Modulab XM ECS (Solartron Analytical), was used for all electrochemical measurements. An area of 9.62 cm^2 (diameter: 35 mm) of the working and counter electrodes was exposed to the electrolyte solution.

H-termination treatments of the BDD electrodes were performed by exposing them to the hydrogen plasma generated by the MWPCVD system (AX6500X) at a 2 kW microwave voltage, chamber pressure of 30 Torr, and hydrogen gas flow rate of 300 sccm. Oxygen- (O-) termination treatments of the BDD electrodes were performed via anodic oxidation using cyclic voltammetry (10 cycles between potentials of −3.5 and 3.5 V and then 20 cycles between potentials of 0 and 3.5 V at a scan rate of 1 V s^{-1} in a 0.1 M H_2SO_4 aqueous solution).

After H- and O-termination treatments, the surfaces of BDD electrodes were characterized with X-ray photoelectron spectroscopy (XPS, JPS-9010TR, JEOL Ltd.). The Mg Kα line was used with a pass energy of 10.0 eV. The C 1s spectra were deconvoluted with Gaussian−Lorentzian sum functions after the subtraction of Shirley background using SpecSurf: Analysis, a package of JEOL XPS software. Four peaks deconvoluted from the C 1s spectra were assigned to the following components: 284.0 eV (C−H bond), 284.8 eV (sp^3 C−C), 285.5 eV (C−O bond), and 286.3 eV (C═O bond).

The surface roughnesses of H- and O-terminated BDD samples were evaluated by using a confocal 3D laser scanning microscope (VK-X1000, KEYENCE CORPORATION.). Three-dimensional roughness parameters S_a and S_z were estimated from the 100 μm × 80 μm area in 3D-images of BDD surfaces.

Cyclic voltammetry (CV) and electrochemical impedance spectroscopy (EIS) were performed with 1 mM $K_4[Fe(CN)_6]$ dissolved in 1 M KCl. The cyclic voltammograms were collected in the potential range from −0.4 to 0.8 V (vs Ag/AgCl) at scan rates of 10, 20, 50, 100, and 200 mVs^{-1}. The EIS spectra were collected in the frequency range of 10 kHz to 0.1 Hz with a voltage amplitude of 10 mV and a bias voltage of 0 V vs open circuit. All cyclic voltammograms and EIS spectra were collected after degassing the electrolyte solutions by nitrogen bubbling. EIS spectra were analyzed using ZView 4.0, a software package for analysis of EIS measurements (Scribner Associates, Inc.).

2.4. Construction of BDD Mesa Structures and Measurements of Electrical Properties of the BDDs

An inductively coupled plasma reactive ion etching system (ELIONIX ELS-7000) was used to dry-etch the BDD layer to construct mesa structures. O-Terminated 0.1%BDD samples on Si and Mo substrates were partially masked with Al tape to afford 5 and 1 mm squares (Figure S13a). The samples were then etched by exposing them to O_2/CF_4 plasma for 90 min (Figure S13b). Subsequently, Al tape was removed from the samples. The mesa-structured BDD samples on the Si and Mo substrates were cleaned with hot mixed acid (H_2SO_4/HNO_3 = 3/1) and acetone, respectively (Figure S13c).

The current−voltage (I−V) characteristics of the 2-in. BDD electrodes and BDD mesa-structures were evaluated with a manual probe equipped with two gold spring probes for electrical contact with the BDD electrode surface. The I−V curves were collected in the voltage range from −8.0 to 8.0 V using an electrochemical station, Modulab XM ECS (Solartron Analytical).

https://doi.org/10.1021/jacsau.4c00006
JACS Au 2024, 4, 1184−1193

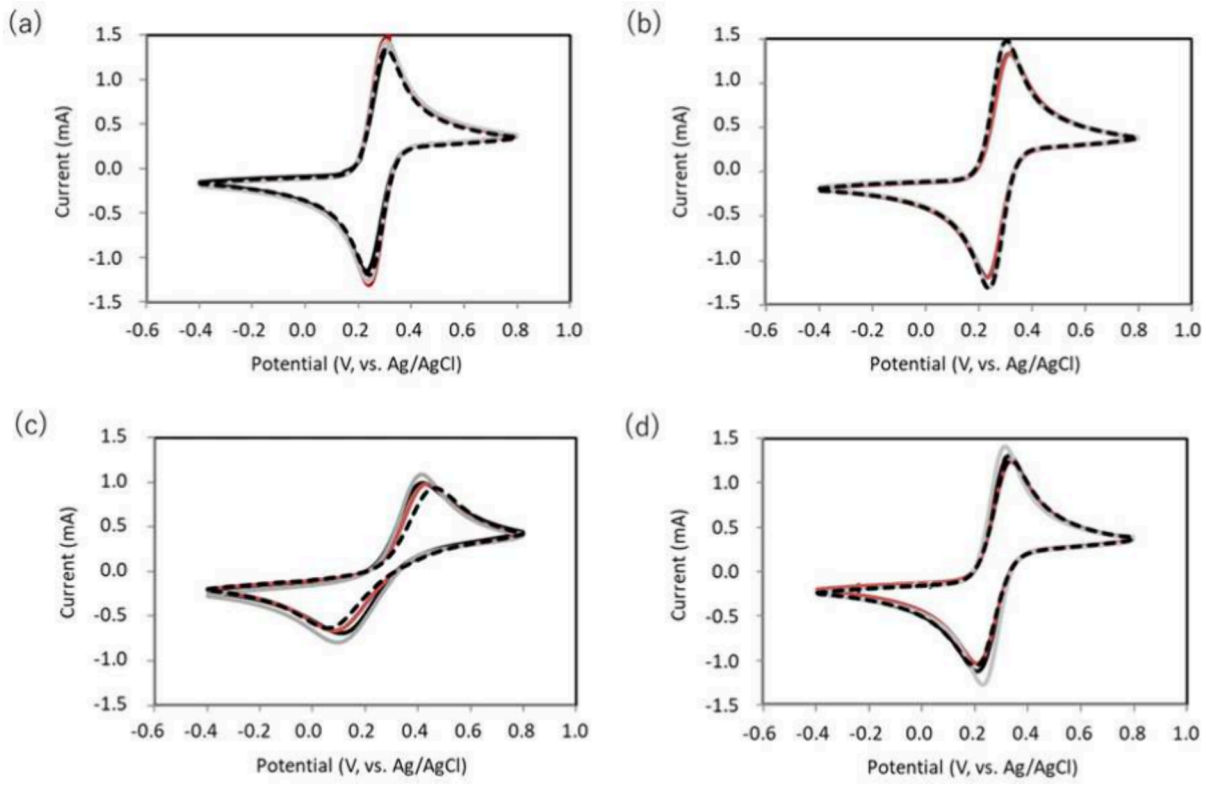

Figure 1. Cyclic voltammograms of $Fe(CN)_6^{3-/4-}$ with H-terminated (a) 0.1%BDD and (b) 1.0%BDD and O-terminated (c) 0.1%BDD and (d) 1.0%BDD on Si (solid black line), W (solid red line), Nb (solid gray line), and Mo (dashed line) substrates.Abbreviations: BDD, boron-doped diamond.

The capacitance−voltage ($C-V$) characteristics of the BDD mesa structures were evaluated with a vacuum prober station (Nagase Techno-Engineering Co., Ltd.) equipped with a high resistance electrometer, Keysight B2985A and a precision LCR meter, Agilent E4980A. The $C-V$ curves were obtained at a frequency of 1000 Hz in the voltage range from −1.0 to 1.0 V.

3. RESULTS AND DISCUSSION

3.1. Electrochemical Properties of BDD Electrodes

In this section, we experimentally investigated the effects of surface termination, the boron-doping level, and the substrate material. First, BDD electrodes were prepared on a p-type single-crystalline Si substrate (0.005−0.01 Ω·cm) as well as W, Nb, and Mo substrates. The boron-doping amount was controlled by using B/C atomic ratios of 0.1% and 1.0% in the CVD feed gas mixture, where the resultant BDD types were denoted as 0.1%BDD and 1.0%BDD, respectively. The boron concentrations in 0.1%BDD and 1.0%BDD were estimated to be 3.3×10^{20} and 1.9×10^{21} cm^{-3}, respectively, via secondary ion mass spectroscopy (SIMS) and glow discharge optical emission spectrometry (GDOES).[55,65] The BDD films were pretreated to obtain H- and O-terminations prior to performing their electrochemical measurements. The effect of H- and O-termination treatments were confirmed by XPS measurement and analysis of C 1s narrow scan peaks as summarized in Figure S1 and Table S1.

To investigate the redox behavior of the BDD electrodes, CV and EIS were performed using the typical redox couple ferri/ferrocyanide ($Fe(CN)_6^{3-/4-}$) in a 1 M KCl aqueous electrolyte. $Fe(CN)_6^{3-/4-}$ typically shows reversible redox behavior with various electrode materials including BDD electrodes.[66] The redox behavior of $Fe(CN)_6^{3-/4-}$ is known to be influenced by surface termination of BDD electrodes.[50,55,56]

Figure 1 shows the cyclic voltammograms of $Fe(CN)_6^{3-/4-}$ with 0.1%BDD and 1.0%BDD synthesized on various substrate materials at a scan rate of 50 mVs^{-1}. The CV measurements at other scan rate (10, 20, 100, and 200 mVs^{-1}) are shown in Figures S2 and S3. The H-terminated 0.1%BDD and 1.0% BDD exhibited comparable cyclic voltammograms, regardless of the boron-doping levels and substrate materials (Figures 1a and b). However, the O-terminated 0.1%BDD showed an obvious increase in peak separation (ΔE_p) (Figure 1c). In addition, the O-terminated 1.0%BDD exhibited ΔE_p smaller than that of 0.1%BDD (Figure 1d).

The peak separation (ΔE_p) and peak current (I_{pa}, I_{pc}) with each CV of BDD electrodes are summarized in Tables S2−S5 and Figure S4. H-0.1% and 1.0%BDD and O-1.0%BDD showed ΔE_p close to the theoretical value (59 mV)[67] in the small sweep rate, while ΔE_p increased along with the sweep rate. And the ratios of anodic and cathodic peak current ($[I_{pa}]/[I_{pc}]$) were close to 1.0. This indicated that these BDD behaved as quasi-reversible electrodes with $Fe(CN)_6^{3-/4-}$. Notably, 0.1%BDD showed a much larger value in ΔE_p and $[I_{pa}]/[I_{pc}]$. This indicates the irreversible behaviors of the O-terminated 0.1%BDD with $Fe(CN)_6^{3-/4-}$. This finding suggests that the CVs of BDD are influenced by the surface termination and boron-doping levels, but not by the substrate material.

Typically, the current measured in a CV is affected by the rates of electron transfer at the electrode−electrolyte interface and the mass transfer of the redox species.[67] As all CV measurements were performed under the same conditions

https://doi.org/10.1021/jacsau.4c00006
JACS Au 2024, 4, 1184−1193

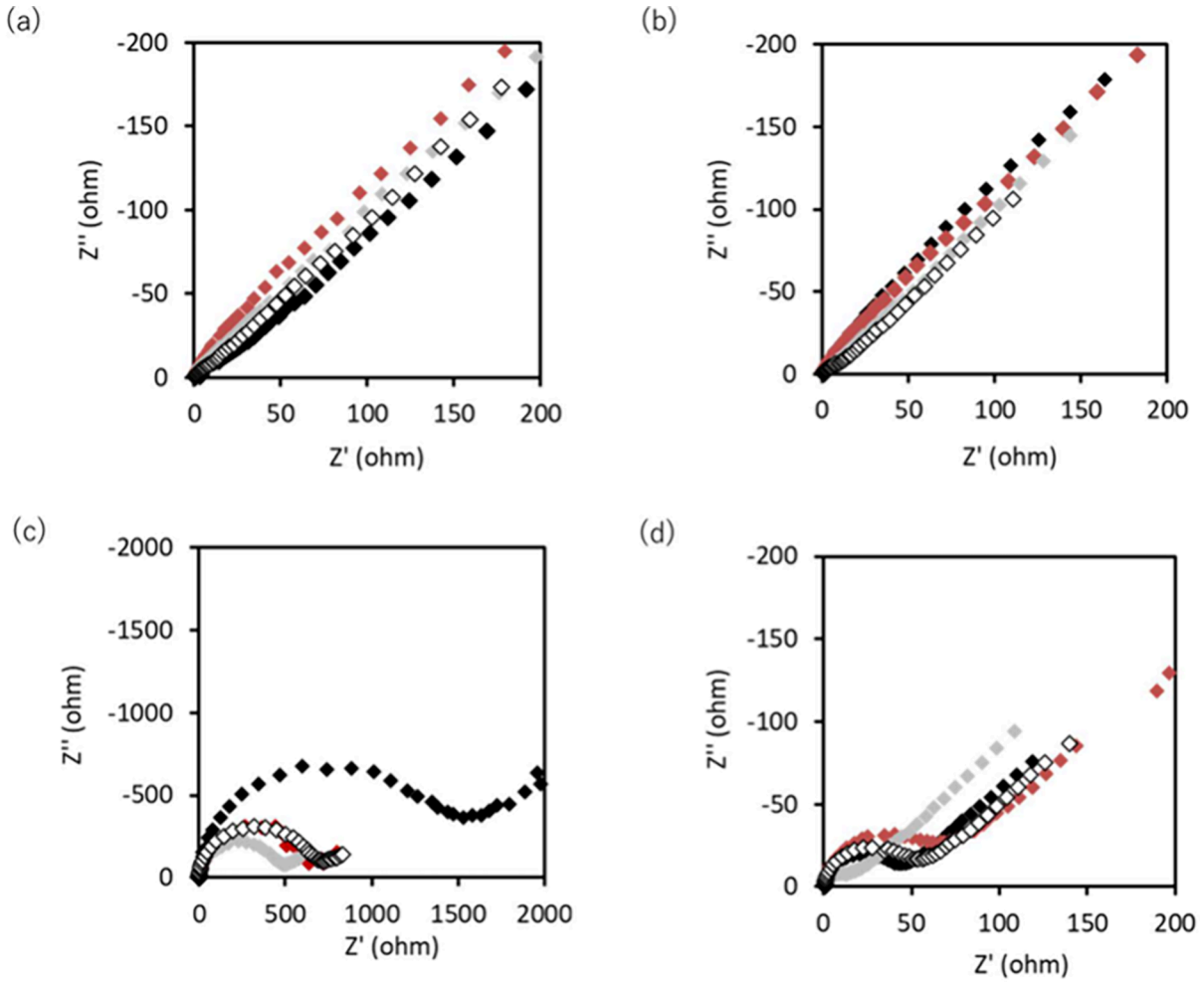

Figure 2. Nyquist plots of $Fe(CN)_6^{3-/4-}$ with H-terminated (a) 0.1%BDD and (b) 1.0%BDD and O-terminated (c) 0.1%BDD and (d) 1.0%BDD on Si (black tilted square), W (red tilted square), Nb (gray tilted square), and Mo (open tilted square) substrates.

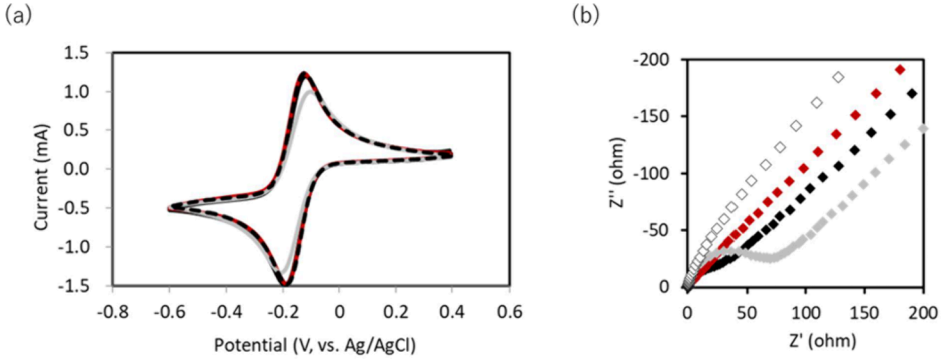

Figure 3. (a) Cyclic voltammograms of $Ru(NH_3)_6^{2+/3+}$ with H-0.1%BDD/Si (solid black line), H-1.0%BDD/Si (solid red line), O-0.1%BDD/Si (solid gray line), and H-0.1%BDD/Si (dashed line). (b) Nyquist plots of of $Ru(NH_3)_6^{2+/3+}$ with H-0.1%BDD/Si (black tilted square), H-1.0% BDD/Si (red tilted square), O-0.1%BDD/Si (gray tilted square), and H-1.0%BDD/Si (open tilted square).

except for the working electrode, the mass transfer of $Fe(CN)_6^{3-/4-}$ in the electrolyte solution should be comparable. Thus, the change in the shape of the CVs in Figure 1c and the increase in ΔE_p can be attributed to the reduced rates of electron transfer in the BDD electrodes.

Electrochemical impedance spectroscopy (EIS) is a powerful tool to analyze the kinetics of electrochemical reactions. As previous studies have not investigated the effects of Si and metal substrates in detail,[23,49,58,59,68] we obtained the EIS spectra of the BDD electrodes to investigate the charge and mass transfer separately.

Figure 2 shows the Nyquist plots of 0.1% and 1.0%BDD deposited on Si, W, Nb, and Mo substrates. The H-terminated BDDs exhibited identical Nyquist plots regardless of the boron-doping level and substrate material (Figures 2a and b). This finding is consistent with their reversible CV behaviors (Figures 1a and b) and the EIS measurements reported by Long et al.[58] The linear plots with a slope of 45° of the H-

https://doi.org/10.1021/jacsau.4c00006
JACS Au 2024, 4, 1184−1193

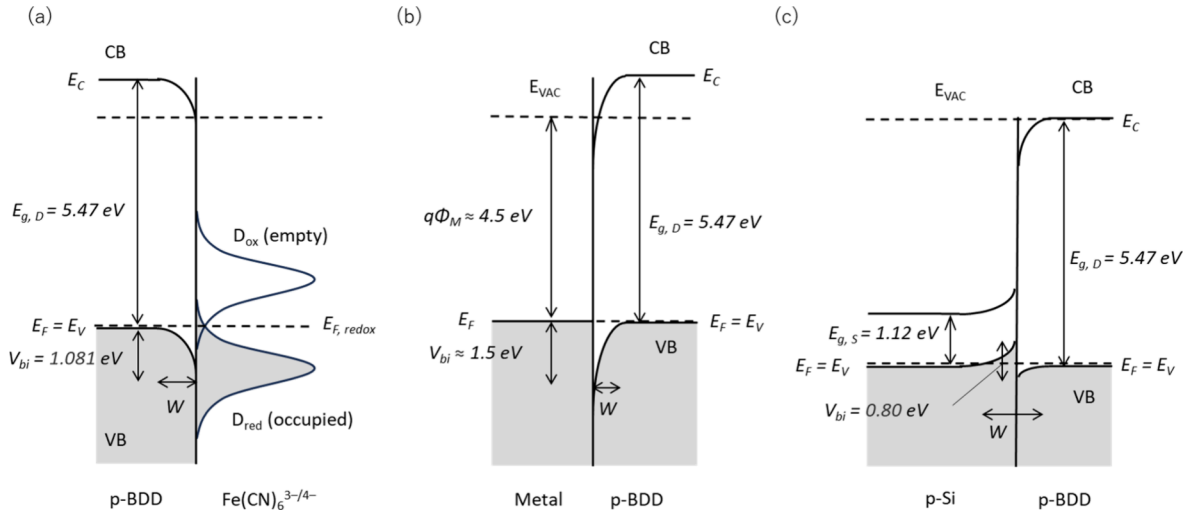

Figure 4. Proposed band diagrams of the (a) p-BDD/electrolyte interface, (b) metal/p-BDD Schottky junction, and (c) p-Si/p-BDD anisotropic heterojunction.

terminated BDDs exhibited negligible charge transfer resistance, and the electrode reaction corresponds to a typical diffusion control model.[69]

In contrast, the O-terminated BDDs exhibited a semicircle trend in the high-frequency region, which indicates decelerated electron transfer at the electrode/electrolyte interface. The Nyquist plot of the O-terminated 0.1%BDD (Figure 2c) indicates an influence of the substrate material, which is not observed in their cyclic voltammograms (Figure 1c). The diameters of semicircles in Nyquist plots are interpreted as the relative charge transfer resistances, where 0.1%BDD exhibited its resistances (>500 Ω) much larger than those of 1.0%BDD (∼50 Ω). This finding is consistent with their different relative peak separations (ΔE_p) in Figures 1c and d. Notably, 0.1% BDD/Si exhibited a charge transfer resistance (∼1500 Ω) larger than that of the 0.1%BDDs with metal substrates.

Figure S5 shows the corresponding Nyquist plots zoomed into high frequency regions. The series of resistances (R_s) can be determined from the high frequency limit of each Nyquist plot. R_s includes solution resistance, substrate resistance, contact resistance between substrates and current collectors (Cu plates), and interfacial resistances between electrolyte/BDD and BDD/substrates. The R_s seems larger in BDD synthesized on Si substrates, which can be attributed to the Si substrates. But the further clarification is needed to understand the influence of R_s on the electrochemical properties.

Additionally, CV and EIS were performed using another redox couple, $Ru(NH_3)_6^{2+/3+}$ in a 1 M KCl aqueous electrolyte. $Ru(NH_3)_6^{2+/3+}$ was reported as an outer-sphere redox active species and not sensitive with the surface termination of BDD electrodes.[50,70] The CV is shown in Figures 3a and S6 and summarized in Table S6 and Figure S7. The results showed that $Ru(NH_3)_6^{2+/3+}$ exhibited reversible or quasi-reversible behaviors with all BDD electrodes. However, a slight increase of ΔE_p observed in the CV of O-0.1%BDD indicated the decelerated electron transfer between the BDD surface and $Ru(NH_3)_6^{2+/3+}$ (Figure 3a). The Nyquist plots of O-0.1%BDD with $Ru(NH_3)_6^{2+/3+}$ also showed increasing of the charge transfer resistance at the BDD/electrolyte interface (Figure 3b). The results suggested that the rate of electron transfer depends on the redox species, but the same trend observed in electrochemical measurements with $Fe(CN)_6^{3-/4-}$ and $Ru(NH_3)_6^{2+/3+}$ confirmed the influence of the substrate of BDD electrodes as well as surface termination and boron-doping level.

3.2. Interpretation of the Electrochemical Behavior of BDD Electrodes

In this section, we compare the electrochemical behaviors of the BDD electrodes (Nyquist plots in Figure 2), which were influenced by the surface terminations, boron concentrations, and substrate materials with those in the literature to explain the observed trends.

Hens reported an equivalent circuit to explain the surface state-mediated electron transfer of semiconductor electrodes, which includes charge transfer at the electrode−electrolyte interface and mass transfer via diffusion process.[71] According to the Hens's model, a linear plot with a 45° slope is anticipated if the charge transfer resistance is assumed to be extremely small.[70]

The surface states of H-terminated diamond demonstrate surface conductivity through acceptor-like surface states,[11,13] which are stabilized by anions such as chloride (Cl^-).[72] Thus, the Nyquist plots of our H-terminated BDDs (Figures 2a and b) suggest negligible charge transfer resistance at the electrode/electrolyte interface, where the impedance is associated with diffusion process. In addition, these plots (Figures 2a and b) are comparable regardless of the boron-doping level and substrate material, suggesting that H-terminated BDD experiences surface state-mediated rapid electron transfer with a small charge transfer resistance. Moreover, as the surface states are generated due to the difference of electronegativity between C and H atoms, the surface-state-mediated electron transfer is not affected by the boron-doping levels or substrate materials. Sachsenhauser et al. also reported a model of the surface state-mediated electron transfer.[73] Based on Sachsenhauser's model, a possible band diagram and electron transfer mechanism of H-terminated BDD is described in Figure S8.

O-Terminated BDD shows different trends in the Nyquist plots (Figures 2c and d). As BDDs are p-type semiconductors, band bending along with the generation of depletion layers occurs due to the electron transfer between the semiconductor electrodes and redox species in the electrolyte solution (Figure

https://doi.org/10.1021/jacsau.4c00006
JACS Au 2024, 4, 1184−1193

4a) The depletion layer width (W) is calculated by eq 1, which is derived from the Poisson equation.[74]

$$W = \sqrt{\frac{2\varepsilon V_{bi}}{qN_A}} \quad (1)$$

where ε, V_{bi}, q, and N_A are the dielectric constant of diamond, the built-in potential, the elementary charge, and the acceptor concentration, respectively. As the 0.1% and 1.0%BDD contain high carrier concentrations ($N_A > 1 \times 10^{20}$ cm^{-3}), the Fermi level is assumed to be incorporated into the valence band maximum ($E_F = E_V$).[21,75] In this model, the built-in potential (V_{bi}) is calculated from the electron affinity ($q\chi_D$) and the bandgap ($E_{g,D}$) of the diamond, and the Fermi level of the redox species ($E_{F,redox}$) is expressed as follows:

$$V_{bi} = (q\chi_D + E_{g,D}) - E_{F,redox} \quad (2)$$

In addition, $E_{F,redox}$ is expressed in terms of the standard redox potential of the redox species based on the vacuum level (U^V_{redox}) and the standard hydrogen electrode (U^0_{redox}) as follows:[76]

$$E_{F,redox} = -qU^V_{redox} = -q(U^0_{redox} + 4.44) \quad (3)$$

The depletion layer width (W) was calculated to be 1.4 and 0.6 nm for of 0.1%BDD and 1.0%BDD, respectively, based on the following values from the literature: $q\chi_D$ = 0.5 eV, $E_{g,D}$ = 5.47 eV, and U^0_{redox} = 0.449 eV.[77−79] Notably, 0.1%BDD has a lower carrier concentration and a larger depletion width, which contribute to the large charge transfer resistance. The proposed band diagram (Figure 4a) rationally explains the different charge transfer resistances of O-terminated 0.1%BDD (>500 Ω) and 1.0%BDD (∼50 Ω) observed in their Nyquist plots (Figures 2c and d).

Moreover, the electrochemical behavior of the O-terminated 0.1%BDD is influenced by the substrate material. The 0.1% BDD on the Si substrate exhibited a larger charge transfer resistance (∼1500 Ω) than those on the metal substrates (∼500 Ω) (Figure 2c). The CVD gas composition and all CVD parameters were identical during the preparation of all BDDs. Furthermore, all 0.1%BDDs exhibited identical Raman spectra, indicating identical composition (Figure S9a−d). The SEM images (Figure S10a−d) of the BDDs showed comparable grain sizes with small differences in the facet distribution. Although the (100) and (111) facets of single-crystalline BDDs exhibited different reactivities,[80,81] the influences of small differences in the facet distributions of are not observed in CV and EIS (Figures 1 and 2). Additionally, surface roughness of the BDD electrodes were evaluated (Figure S11). The larger roughness of BDD electrodes synthesized on metal substrates originates from scratches created by sandpaper polishing of metal substrates for the seeding of BDD growth. The data showed almost no change of surface roughness after H-termination and O-termination of the 0.1%BDD/Si. Therefore, the difference observed in Figure 2c is attributed to the diamond−substrate interface.

The 0.1%BDDs synthesized on metal substrates comprise metal−semiconductor junctions. The work functions ($q\Phi_M$) of W, Nb, and Mo are 4.5, 4.3, and 4.6 eV, respectively.[82] These work functions of metals, and electron affinity ($q\Phi_D$ = 0.5 eV) and bandgap of diamond ($E_{g,D}$ = 5.47 eV)[77,78] suggest the possibility of Schottky contacts between the BDD and metal substrates. Assuming the formation of Schottky contact, we propose a possible band diagram for the metal/p-BDD interface (Figure 4b). Band bending occurs at the interface due to the Fermi level difference between the metals and BDD, generating depletion layers. The depletion layer width (W) was calculated by using eq 2. As the model in which the Fermi level incorporated into the valence band maximum was employed as shown in Figure 3b, built-in potentials (V_{bi}) can be expressed as follows:

$$V_{bi} = (q\chi_D + E_{g,D}) - q\Phi_M \quad (4)$$

The depletion layer widths with the W, Nb, and Mo substrates were calculated to be 1.4, 1.7, and 1.4 nm, respectively, using eqs 1 and 4.

BDD synthesized on a Si substrate comprises semiconductor heterojunctions at the interface, which generate energy barriers called band discontinuities.[60−63] As both BDD and the conductive Si used in this study are p-type semiconductors, we propose a band diagram for p-/p-anisotropic heterojunction at the p-Si/p-BDD interface (Figure 4c).[83] Semiconductor heterojunctions also form depletion layers (Figure 4b). The depletion layer width (W) and the energy barrier height (V_{bi}) are expressed as eqs 5[83,84] and 6 when the Fermi level is incorporated into the valence band maximum ($E_F = E_V$):

$$W = \sqrt{\frac{2\varepsilon_{Si}\varepsilon_D V_{bi}(N_{Si}{}^2 + N_D{}^2)}{q(\varepsilon_{Si}N_{Si} + \varepsilon_D N_D)N_{Si}N_D}} \quad (5)$$

$$V_{bi} = (q\chi_D + E_{g,D}) - (q\Phi_{Si} + E_{g,Si}) \quad (6)$$

where q is the elementary charge, ε_{Si}, ε_D, N_{Si}, N_D, $q\Phi_{Si}$, $q\Phi_D$, $E_{g,Si}$, and $E_{g,D}$ are dielectric constants, acceptor concentrations, electron affinities, band gaps of Si and diamond, respectively. The energy barrier height (V_{bi}) is calculated to be 0.80 eV using $q\Phi_D$, $E_{g,D}$, $q\Phi_{Si}$, and $E_{g,Si}$ from the literature.[77,78,83] The estimated depletion width (W) of 0.1%BDD/Si was 10.0 nm, which is much larger than those of 0.1%BDD/metals (1.4−1.7 nm). The larger W could have contributed to the larger charge transfer resistance of 0.1%BDD/Si (∼1500 Ω) than that of 0.1%BDD/metals (∼500 Ω).

3.3. Electrical Properties of 0.1%BDD Electrodes

We aimed to validate the electrochemical behaviors and proposed band diagrams by obtaining the electrical properties of the BDD electrodes synthesized by using different substrate materials. First, we obtained the $I-V$ curves of the BDD films synthesized on 2-in. substrates. Two spring probes were attached to the surface of the BDDs and the applied DC voltages (Figure S12). The conductivity of BDD was influenced by the boron-doping levels and substrate materials. In particular, 1.0%BDD exhibited higher conductivity than 0.1%BDD for all substrates (Figure 5). Although the conductivities of both 1.0%BDD/Si and 0.1%BDD/Si were lower than those of the BDD/metal substrates, this trend is more pronounced in 0.1%BDD. In addition, 0.1%BDD was synthesized on an ALO substrate, which demonstrated an even lower current than that of the BDD/Si electrodes (Figure 5). This confirms that the conductivity of the substrate materials influences the conductivity of the BDD electrodes.

Next, we fabricated BDD mesa structures with O-terminated 0.1%BDD/Si to clarify the conduction mechanism (Figure S13). The mesa structures comprised several 5 and 1 mm squared BDD pads. Figure 6 shows the $I-V$ curves of the mesa

https://doi.org/10.1021/jacsau.4c00006
JACS Au 2024, 4, 1184−1193

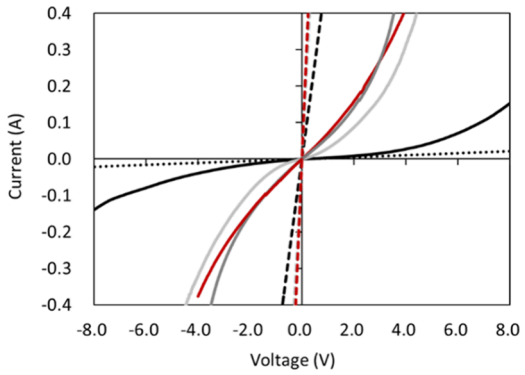

Figure 5. *I*−*V* characteristics of 1.0%BDD/Si (black dashed line), 1.0%BDD/W (red dashed line), 1.0%BDD/Nb (dark gray dashed line), 1.0%BDD/Mo (light gray dashed line), 0.1%BDD/Si (black solid line), 0.1%BDD/W (red solid line), 0.1%BDD/Nb (dark gray solid line), 0.1%BDD/Mo (light gray solid line), and 0.1%BDD/ALO (dotted line).

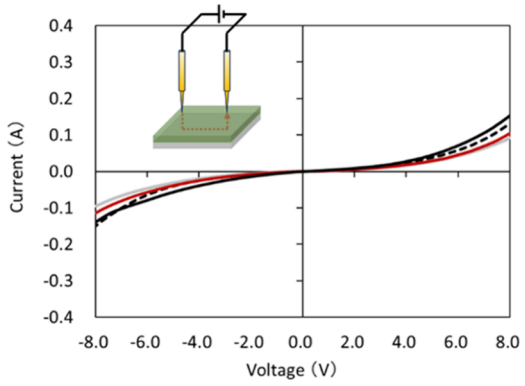

Figure 6. *I*−*V* curves of single-pad φ2 in. (black solid line), 5 mm square (red solid line), and 1 mm square (gray solid line), as well as dual-pad 1 mm square (dashed line), 0.1%BDD electrodes on Si substrates.

structures. First, *I*−*V* curves were collected using single BDD pads of different sizes (Figure S14a). All *I*−*V* curves were almost identical (Figure 6). Subsequently, *I*−*V* curves of dual pads were obtained (Figure S14b). These *I*−*V* curves were also identical with those of single pads. This suggests that conduction predominantly occurs through the BDD/Si interface and Si substrate and not the horizontal direction (Figure 6).

The proposed band discontinuities created by the p-Si/p-BDD semiconductor heterojunction are shown in Figure 4c. The *I*−*V* curves of the 0.1%BDD mesa structures revealed the BDD/Si interface and the Si substrate as the main conduction routes. Hence, the depletion layer capacitance is anticipated at the p-Si/p-BDD interface. To demonstrate the validity of the proposed band diagram and the conduction pathway, we evaluated the capacitance−voltage (*C*−*V*) characteristics of the Si and Mo BDD mesa structures. Two spring probes were attached to the BDD and substrate surfaces (Figure S15a). An AC voltage was applied at a frequency of 1000 Hz with a DC voltage from −1.0 to 1.0 V to investigate the voltage dependency. The capacitance of the Si surface was used as the baseline (Figure S15b). The capacitances of 0.1%BDD/Si and 0.1%BDD/Mo were significantly and slightly larger than that of the baseline, whereas the capacitance of 1.0%BDD/Si was nearly identical with that of the baseline (Figure 7). As the

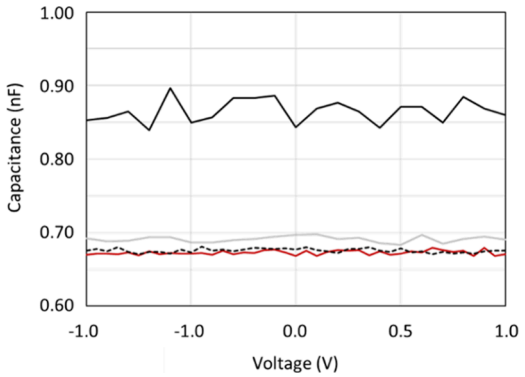

Figure 7. *C*−*V* plots of O-terminated 0.1%BDD/Si (black solid line), 1.0%BDD/Si (red solid line), 0.1%BDD/Mo (gray solid line), and baseline (dashed line) BDD mesa-structures.

BDD mesa-structured samples for *C*−*V* measurements were O-terminated, *C*−*V* characteristics of H-terminated BDD are also of interests. But the method of capacitance measurement is not sensitive enough to distinguish H- and O-termination of BDD samples. The further investigation for the improving surface sensitivity is undergoing.

The larger capacitance of 0.1%BDD/Si shown in Figure 7 is attributed to the larger electron transfer resistance observed in the Nyquist plot (Figure 2c). The depletion layer widths of 0.1%BDD on Mo and Si substrates were estimated to be 1.4 and 10.0 nm, respectively. The large depletion layer width of the Si substrate could have increased the capacitance of 0.1% BDD/Si, thus influencing its electrochemical properties. Moreover, the interfacial capacitance and charge transfer resistance of 1.0%BDD/Si did not increase (Figure 7), despite the generation of a large depletion layer width (10.2 nm). This suggests that the BDD/Si interface is not involved in the conduction mechanism at high boron-doping levels. Furthermore, the high carrier concentrations of highly doped BDD likely contribute to reducing the charge transfer at the electrode/electrolyte interface.

An equivalent circuit has been previously proposed to explain the electron transfer at the interface of the semiconductor electrode and the electrolyte.[71,85] In this study, we propose a new equivalent circuit by considering the substrate and the substrate-electrode interface (Figure 8). The new equivalent circuit will explain the influence of the substrate materials and substrate/BDD interfaces on the electron transfer at the electrode/electrolyte interface. In this model, O-terminated BDDs exhibit depletion layer resistances at the electrode/electrolyte interfaces (R_{SC}). In addition, the boron-doping levels could explain the differences in the depletion layer capacitances (C_{SC}) and resistances (R_{SC}) at the electrode/electrolyte interfaces. The different electrochemical behaviors of O-terminated 0.1%BDD on Si and metal substrates (Figure 2c) are explained by the differences in the depletion layer capacitances ($C_{Sub/BDD}$) and resistances ($R_{Sub/BDD}$) due to the substrate materials.

The EIS spectra shown in Figure 2 were simulated by using this equivalent circuit. The simulated EIS spectra showed good fitting with the corresponding experimental spectra (Figures S16−S19). The simulated values for each component are summarized in Table S7. As expected, O-0.1%BDD exhibits larger $R_{Sub/BDD}$ and R_{SC}, particularly with the Si substrate. The results supported the validity of the proposed equivalent circuit.

https://doi.org/10.1021/jacsau.4c00006
JACS Au 2024, 4, 1184−1193

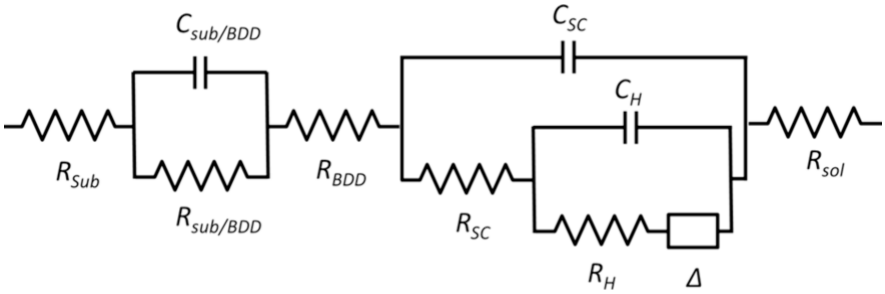

Figure 8. Proposed equivalent circuit considering the BDD/electrolyte and BDD/substrate interfaces.

4. CONCLUSION

In this study, we experimentally and theoretically investigated the influence of the substrate materials on the electrical properties of boron-doped diamonds (BDD). Oxygen-terminated BDD/Si with moderate boron-doping levels exhibited sluggish electron transfer induced by the large capacitance generated at the BDD/Si substrate. Band diagrams were proposed considering BDD as a p-type semiconductor to understand the electron transfer at the BDD/electrolyte and substrate/BDD interfaces. Metal-like ohmic behaviors of the highly doped BDDs were explained by the small width of the depletion layers at the BDD/electrolyte interfaces. The different band structures generated at the metal−semiconductor junctions and semiconductor heterojunctions of the BDD electrodes resulted in different electrochemical properties. This study provides a fundamental understanding of diamond electrochemistry and new insights into the appropriate selection of substrate materials for practical applications of BDD electrodes.

■ ASSOCIATED CONTENT

Supporting Information

The Supporting Information is available free of charge at https://pubs.acs.org/doi/10.1021/jacsau.4c00006.

Supplemental Figures and Tables regarding characterizations and electrochemical properties of the BDD electrodes and the procedures for the electrical measurements (PDF)

■ AUTHOR INFORMATION

Corresponding Author

Yasuaki Einaga − *Department of Chemistry, Keio University, Yokohama 223-8522, Japan;* orcid.org/0000-0001-7057-4358; Phone: +81-45-566-1704; Email: einaga@chem.keio.ac.jp; Fax: +81-45-566-1697

Authors

Atsushi Otake − *Department of Chemistry, Keio University, Yokohama 223-8522, Japan*

Taiki Nishida − *Sensing Material Research Team, Sensing System Research Center, National Institute of Advanced Industrial Science and Technology, Tosu, Saga 841-0052, Japan*

Shinya Ohmagari − *Sensing Material Research Team, Sensing System Research Center, National Institute of Advanced Industrial Science and Technology, Tosu, Saga 841-0052, Japan*

Complete contact information is available at: https://pubs.acs.org/10.1021/jacsau.4c00006

Author Contributions

A.O. designed and performed the experiments and wrote the original draft. T.N. performed the experiments. A.O., T.N., S.O., and Y.E. analyzed the results. All authors edited the manuscript. CRediT: **Atsushi Otake** conceptualization, data curation, formal analysis, investigation, writing-original draft, writing-review & editing; **Taiki Nishida** investigation, methodology, writing-review & editing; **Shinya Ohmagari** methodology, validation, writing-review & editing; **Yasuaki Einaga** formal analysis, funding acquisition, investigation, supervision, writing-review & editing.

Notes

The authors declare no competing financial interest.

■ ACKNOWLEDGMENTS

This work was partially supported by the New Energy and Industrial Technology Development Organization (NEDO) P16002 (Y.E.), and the Grant-in-Aid for Scientific Research A 23H00288 (Y.E.).

■ REFERENCES

(1) *Power Electronics Device Applications of Diamond Semiconductors*; Koizumi, S., Umezawa, H., Pernot, J., Suzuki, M., Eds.; Elsevier, 2018. DOI:

(2) Wort, C. J. H.; Balmer, R. S. Diamond as an electronic material. *Mater. Today* **2008**, *11* (1−2), 22−28.

(3) Donato, N.; Rouger, N.; Pernot, J.; Longobardi, G.; Udrea, F. Diamond power devices: State of the art, modelling, figures of merit and future perspective. *J. Phys. D: Appl. Phys.* **2020**, *53* (9), No. 093001.

(4) Umezawa, H. Recent advances in diamond power semiconductor devices. *Mater. Sci. Semicond. Process.* **2018**, *78*, 147−156.

(5) Dang, C.; Lu, A.; Wang, H.; Zhang, H.; Lu, Y. Diamond semiconductor and elastic strain engineering. *J. Semicond.* **2022**, *43* (2), No. 021801.

(6) *Diamond Electrochemistry*, 1st ed.; Fujishima, A., Einaga, Y., Rao, T. N., Tryk, D. A., Eds.; Elsevier, 2005.

(7) Einaga, Y.; Foord, J. S.; Swain, G. M. Diamond electrodes: Diversity and maturity. *MRS Bull.* **2014**, *39* (6), 525−532.

(8) Yang, N.; Yu, S.; Macpherson, J. V.; Einaga, Y.; Zhao, H.; Zhao, G.; Swain, G. M.; Jiang, X. Conductive diamond: synthesis, properties, and electrochemical applications. *Chem. Soc. Rev.* **2019**, *48* (1), 157−204.

(9) Yu, S.; Liu, S.; Jiang, X.; Yang, N. Recent advances on electrochemistry of diamond related materials. *Carbon* **2022**, *200*, 517−542.

(10) Landstrass, M. I.; Ravi, K. V. Hydrogen passivation of electrically active defects in diamond. *Appl. Phys. Lett.* **1989**, *55* (14), 1391−1393.

(11) Kawarada, H. Hydrogen-terminated diamond surfaces and interfaces. *Surf. Sci. Rep.* **1996**, *26* (7), 205−206.
(12) Hayashi, K.; Yamanaka, S.; Okushi, H.; Kajimura, K. Study of the effect of hydrogen on transport properties in chemical vapor deposited diamond films by Hall measurements. *Appl. Phys. Lett.* **1996**, *68* (3), 376−378.
(13) Maier, F.; Riedel, M.; Mantel, B.; Ristein, J.; Ley, L. Origin of surface conductivity in diamond. *Phys. Rev. Lett.* **2000**, *85* (16), 3472−3475.
(14) Crawford, K. G.; Maini, I.; Macdonald, D. A.; Moran, D. A. J. Surface transfer doping of diamond: A review. *Prog. Surf. Sci.* **2021**, *96* (1), No. 100613.
(15) Hirama, K.; Takayanagi, H.; Yamauchi, S.; Yang, J. H.; Kawarada, H.; Umezawa, H. Spontaneous polarization model for surface orientation dependence of diamond hole accumulation layer and its transistor performance. *Appl. Phys. Lett.* **2008**, *92* (11), 112107.
(16) Kawarada, H.; Yamada, T.; Xu, D.; Tsuboi, H.; Kitabayashi, Y.; Matsumura, D.; Shibata, M.; Kudo, T.; Inaba, M.; Hiraiwa, A. Durability-enhanced two-dimensional hole gas of C-H diamond surface for complementary power inverter applications. *Sci. Rep.* **2017**, *7* (1), 42368.
(17) Koizumi, S.; Kamo, M.; Sato, Y.; Mita, S.; Sawabe, A.; Reznik, A.; Uzan-Saguy, C.; Kalish, R. Growth and characterization of phosphorus doped n-type diamond thin films. *Diam. Relat. Mater.* **1998**, *7* (2−5), 540−544.
(18) Kociniewski, T.; Barjon, J.; Pinault, M.-A.; Jomard, F.; Lusson, A.; Ballutaud, D.; Gorochov, O.; Laroche, J. M.; Rzepka, E.; Chevallier, J.; Saguy, C. n-type CVD diamond doped with phosphorus using the MOCVD technology for dopant incorporation. *Phys. Status Solidi (A)* **2006**, *203* (12), 3136−3141.
(19) Kato, H.; Futako, W.; Yamasaki, S.; Okushi, H. Homoepitaxial growth and characterization of phosphorus-doped diamond using tertiarybutylphosphine as a doping source. *Diam. Relat. Mater.* **2004**, *13* (11−12), 2117−2120.
(20) Katamune, Y.; Arikawa, D.; Mori, D.; Izumi, A. Formation of phosphorus-incorporated diamond films by hot-filament chemical vapor deposition using organic phosphorus solutions. *Thin Solid Films* **2019**, *677*, 28−32.
(21) Blase, X.; Bustarret, E.; Chapelier, C.; Klein, T.; Marcenat, C. Superconducting group-IV semiconductors. *Nat. Mater.* **2009**, *8*, 375−382.
(22) Chen, Y.; Ogura, M.; Yamasaki, S.; Okushi, H. Ohmic contacts on p-type homoepitaxial diamond and their thermal stability. *Semicond. Sci. Technol.* **2005**, *20* (8), 860−863.
(23) Ramesham, R. Determination of flatband potential for boron doped diamond electrode in 0.5 M NaCl by AC impedance spectroscopy. *Thin Solid Films* **1998**, *322* (1−2), 158−166.
(24) Lévy-Clément, C. Semiconducting and metallic boron-doped diamond electrode. *Diamond Electrochemistry*, 1st ed.; Elsevier, 2005; pp 80−114.
(25) Nebel, C. E.; Rezek, B.; Shin, D.; Uetsuka, H.; Yang, N. Diamond for bio-sensor applications. *J. Phys. D: Appl. Phys.* **2007**, *40* (20), 6443−6466.
(26) Yang, W.; Auciello, O.; Butler, J. E.; Cai, W.; Carlisle, J. A.; Gerbi, J. E.; Gruen, E. M.; Knickerbocker, T.; Lasseter, T. L.; Russell, J. N., Jr.; Smith, L. M.; Hamers, R. J. DNA-modified nanocrystalline diamond thin-films as stable, biologically active substrates. *Nat. Mater.* **2002**, *1* (7), 253−257.
(27) Einaga, Y. Diamond electrodes for electrochemical analysis. *J. Appl. Electrochem.* **2010**, *40* (10), 1807−1816.
(28) Schreck, M.; Asmussen, J.; Shikata, S.; Arnault, J.-C.; Fujimori, N. Large-area high-quality single crystal diamond. *MRS Bull.* **2014**, *39* (6), 504−510.
(29) Kato, H.; Yamasaki, S.; Okushi, H. n-type doping of (001)-oriented single-crystalline diamond by phosphorus. *Appl. Phys. Lett.* **2005**, *86* (22), 222111.
(30) Yamasaki, S.; Gheeraert, E.; Koide, Y. Doping and interface of homoepitaxial diamond for electronic applications. *MRS Bull.* **2014**, *39* (6), 499−503.
(31) Sartori, A. F.; Fischer, M.; Gsell, S.; Schreck, M. In situ boron doping during heteroepitaxial growth of diamond on Ir/YSZ/Si. *Phys. Status Solidi (A)* **2012**, *209* (9), 1643−1650.
(32) Aida, H.; Oshima, R.; Ouchi, T.; Kimura, Y.; Sawabe, A. In-situ reflectance interferometry of heteroepitaxial diamond growth. *Diam. Relat. Mater.* **2021**, *113*, 108253.
(33) Wei, Q.; Lin, F.; Wang, R.; Zhang, X.; Chen, G.; Hussain, J.; He, D.; Zhang, Z.; Niu, G.; Wang, H.-X. Heteroepitaxy growth of single crystal diamond on Ir/Pd/Al_2O_3 (11−20) substrate. *Mater. Lett.* **2021**, *303* (15), No. 130483.
(34) Zhang, X.; Matsumoto, T.; Nakano, Y.; Noguchi, H.; Kato, H.; Makino, T.; Takeuchi, D.; Ogura, M.; Yamasaki, S.; Nebel, C. E.; Inokuma, T.; Tokuda, N. Inversion channel MOSFET on heteroepitaxially grown free-standing diamond. *Carbon* **2021**, *175* (30), 615−619.
(35) Perez, G.; Maréchal, A.; Chicot, G.; Lefranc, P.; Jeannin, P.-O.; Eon, D.; Rouger, N. Diamond semiconductor performances in power electronics applications. *Diam. Relat. Mater.* **2020**, *110*, No. 108154.
(36) Matsumoto, T.; Kato, H.; Oyama, K.; Makino, T.; Ogura, M.; Takeuchi, D.; Inokuma, T.; Tokuda, N.; Yamasaki, S. Inversion channel diamond metal-oxide-semiconductor field-effect transistor with normally off characteristics. *Sci. Rep.* **2016**, *6*, 31585.
(37) Umezawa, H.; Tatsumi, N.; Kato, Y.; Shikata, S. Leakage current analysis of diamond Schottky barrier diodes by defect imaging. *Diam. Relat. Mater.* **2013**, *40*, 56−59.
(38) Lagrange, J.-P.; Deneuville, A.; Gheeraert, E. Activation energy in low compensated homoepitaxial boron-doped diamond films. *Diam. Relat. Mater.* **1998**, *7* (9), 1390.
(39) Kato, H.; Ogura, M.; Makino, T.; Takeuchi, D.; Yamasaki, S. N-type control of single-crystal diamond films by ultra-lightly phosphorus doping. *Appl. Phys. Lett.* **2016**, *109* (14), 142102.
(40) Bousquet, J.; Klein, T.; Solana, M.; Saminadayar, L.; Marcenat, C.; Bustarret, E. Phase diagram of boron-doped diamond revisited by thickness-dependent transport studies. *Phys. Rev. B* **2017**, *95* (16), No. 161301.
(41) Karasawa, A.; Makino, T.; Traore, A.; Kato, H.; Ogura, M.; Kato, Y.; Takeuchi, D.; Yamasaki, S.; Sakurai, T. Carrier transport mechanism of diamond p^+−n junction at low temperature using Schottky−pn junction structure. *Jpn. J. Appl. Phys.* **2021**, *60* (3), No. 030905.
(42) Lambert, N.; Taylor, A.; Hubik, P.; Bulíř, J.; More-Chevalier, J.; Karaca, H.; Fleury, C.; Voves, J.; Šobáň, Z.; Pogany, D.; Mortet, V. Modeling current transport in boron-doped diamond at high electric fields including self-heating effect. *Diam. Relat. Mater.* **2020**, *109*, No. 108003.
(43) Kukushkin, V. A. Hopping conduction of non metallic heavily doped delta-layers in CVD diamond. *Diam. Relat. Mater.* **2021**, *116*, No. 108373.
(44) Pleskov, Y. V. Electrochemistry of diamond: A review. *Russ. J. Electrochem.* **2002**, *38* (12), 1275−1291.
(45) Swain, G. M.; Ramesham, R. The electrochemical activity of boron-doped polycrystalline diamond thin film electrodes. *Anal. Chem.* **1993**, *65* (4), 345−351.
(46) Einaga, Y. Boron-doped diamond electrodes: Fundamentals for electrochemical applications. *Acc. Chem. Res.* **2022**, *55* (24), 3605−3615.
(47) *Diamond Electrodes Fundamentals and Applications*, 1st ed.; Einaga, Y., Ed.; Springer, 2022.
(48) Alehashem, S.; Chambers, F.; Strojek, J. W.; Swain, G. M.; Ramesham, R. Cyclic voltammetric studies of charge transfer reactions at highly boron-doped polycrystalline diamond thin-film electrodes. *Anal. Chem.* **1995**, *67* (17), 2812−2821.
(49) Becker, D.; Jüttner, K. The impedance of fast charge transfer reactions on boron doped diamond electrodes. *Electrochim. Acta* **2003**, *49* (1), 29−39.

https://doi.org/10.1021/jacsau.4c00006
JACS Au 2024, 4, 1184−1193

(50) Granger, M. C.; Swain, G. M. The influence of surface interactions on the reversibility of ferri/ferrocyanide at boron-doped diamond thin-film Electrodes. *J. Electrochem. Soc.* **1999**, *146* (12), 4551−4558.
(51) Latto, M. N.; Pastor-Moreno, G.; Riley, D. J. The influence of doping levels and surface termination on the electrochemistry of polycrystalline diamond. *Electroanalysis* **2004**, *16* (6), 434−441.
(52) Ryl, J.; Burczyk, L.; Bogdanowicz, R.; Sobaszek, M.; Darowicki, K. Study on surface termination of boron-doped diamond electrodes under anodic polarization in H_2SO_4 by means of dynamic impedance technique. *Carbon* **2016**, *96*, 1093−1105.
(53) Girard, H.; Simon, N.; Ballutaud, D.; Herlem, M.; Etcheberry, A. Effect of anodic and cathodic treatments on the charge transfer of boron doped diamond electrodes. *Diam. Relat. Mater.* **2007**, *16* (2), 316−325.
(54) Simon, N.; Girard, H.; Ballutaud, D.; Ghodbane, S.; Deneuville, A.; Herlem, M.; Etcheberry, A. Effect of H and O termination on the charge transfer of moderately boron doped diamond electrodes. *Diam. Relat. Mater.* **2005**, *14* (3−7), 1179−1182.
(55) Watanabe, T.; Honda, Y.; Kanda, K.; Einaga, Y. Tailored design of boron-doped diamond electrodes for various electrochemical applications with boron-doping level and sp2-bonded carbon impurities. *Phys. Status Solidi (A)* **2014**, *211* (12), 2709−2717.
(56) Kasahara, S.; Natsui, K.; Watanabe, T.; Yokota, Y.; Kim, Y.; Iizuka, S.; Tateyama, Y.; Einaga, Y. Surface hydrogenation of boron-doped diamond electrodes by cathodic reduction. *Anal. Chem.* **2017**, *89* (21), 11341−11347.
(57) Yu, P.; Zhang, J.; Zheng, T.; Wang, T. Influence of boron doped level on the electrochemical behavior of boron doped diamond electrodes and uric acid detection. *Colloids Surf. A: Physicochem. Eng.* **2016**, *494* (5), 241−247.
(58) Long, H.; Hu, H.; Wen, K.; Liu, X.; Liu, S.; Zhang, Q.; Chen, T. Thickness effects on boron doping and electrochemical properties of boron-doped diamond film. *Molecules* **2023**, *28* (6), 2829.
(59) Yang, W.; Tan, J.; Chen, Y.; Li, Z.; Liu, F.; Long, H.; Wei, Q.; Liu, L.; Ma, L.; Zhou, K.; Yu, Z. Relationship between substrate type and BDD electrode structure, performance and antibiotic tetracycline mineralization. *J. Alloys Compd.* **2022**, *890* (15), No. 161760.
(60) Milnes, A. G. *Heterojunctions and Metal Semiconductor Junctions*, 1st ed.; Elsevier, 1972.
(61) Sharma, B. L.; Purohit, R. K. *Semiconductor Heterojunctions*, 1st ed.; Pergamon Press Ltd., 1974.
(62) Franciosi, A.; Walle, C. G. V. Heterojunction band offset engineering. *Surf. Sci. Rep.* **1996**, *25* (1−4), 1−140.
(63) Guo, X.; Yang, B.; Lu, J.; Li, H.; Huang, N.; Liu, L.; Jiang, X. Electrical tailoring of the photoluminescence of silicon-vacancy centers in diamond/silicon heterojunctions. *J. Mater. Chem. C* **2022**, *10* (24), 9334−9343.
(64) Irvin, J. C. Resistivity of bulk silicon and of diffused layers in silicon. *Bell Syst. Technol. J.* **1962**, *41* (2), 387−410.
(65) Xu, J.; Natsui, K.; Naoi, S.; Nakata, K.; Einaga, Y. Effect of doping level on the electrochemical reduction of CO_2 on boron-doped diamond electrodes. *Diam. Relat. Mater.* **2018**, *86*, 167−172.
(66) Macpherson, J. V. A practical guide to using boron doped diamond in electrochemical research. *Phys. Chem. Chem. Phys.* **2015**, *17* (5), 2935−2949.
(67) Bard, A. J.; Faulkner, L. R. *Electrochemical Methods—Fundamentals and Applications*, 2nd ed.; Wiley, 2001.
(68) Živcová, Z. V.; Petrák, V.; Frank, O.; Kavan, L. Electrochemical impedance spectroscopy of polycrystalline boron doped diamond layers with hydrogen and oxygen terminated surface. *Diam. Relat. Mater.* **2015**, *55*, 70−76.
(69) Lazanas, A. C.; Prodromidis, M. I. Electrochemical impedance spectroscopy-A tutorial. *ACS Meas. Sci. Au* **2023**, *3* (3), 162−193.
(70) Hutton, L. A.; Iacobini, J. G.; Bitziou, E.; Channon, R. B.; Newton, M. E.; Macpherson, J. V. Examination of the factors affecting the electrochemical performance of oxygen-terminated polycrystalline boron-doped diamond electrodes. *Anal. Chem.* **2013**, *85* (15), 7230−7240.
(71) Hens, Z. The electrochemical impedance of one-equivalent electrode processes at dark semiconductor|redox electrodes involving charge transfer through surface states. 1. *Theory. J. Phys. Chem. B* **1999**, *103* (1), 122−129.
(72) Song, K.-S.; Sakai, T.; Kanazawa, H.; Araki, Y.; Umezawa, H.; Tachiki, M.; Kawarada, H. Cl^- sensitive biosensor used electrolyte-solution-gate diamond FETs. *Biosens. Bioelectron.* **2003**, *19* (2), 137−140.
(73) Sachsenhauser, M.; Sharp, I. D.; Stutzmann, M.; Garrido, J. A. Surface state mediated electron transfer across the n-type SiC/electrolyte interface. *J. Phys. Chem. C* **2016**, *120*, 6524−6533.
(74) Rajeshwar, K. Photoelectrochemistry, fundamentals and applications. In *Encyclopedia of Applied Electrochemistry*, 1st ed.; Springer, New York, 2014; pp 1550−1556.
(75) Ohmagari, S.; Matsumoto, T.; Umezawa, H.; Mokuno, Y. Ohmic contact formation to heavily boron-doped p+ diamond prepared by hot-filament chemical vapor deposition. *MRS Adv.* **2016**, *1* (51), 3489−3495.
(76) Bard, A. J.; Memming, R.; Miller, B. Terminology in semiconductor electrochemistry and photoelectrochemical energy conversion (Recommendations 1991). *Pure Appl. Chem.* **1991**, *63* (4), 569−596.
(77) Ikeda, T.; Teii, K. Origin of reverse leakage current in n-type nanocrystalline diamond/p-type silicon heterojunction diodes. *Appl. Phys. Lett.* **2009**, *94* (7), No. 072104.
(78) Goto, M.; Amano, R.; Shimoda, N.; Kato, Y.; Teii, K. Rectification properties of n-type nanocrystalline diamond heterjunctions to p-type silicon carbide at high temperatures. *Appl. Phys. Lett.* **2014**, *104* (15), 153113.
(79) Cline, K. K.; McDermott, M. T.; McCreery, R. L. Anomalously slow electron transfer at ordered graphite electrodes: Influence of electronic factors and reactive sites. *J. Phys. Chem.* **1994**, *98* (20), 5314−5319.
(80) Ando, T.; Asai, K.; Macpherson, J.; Einaga, Y.; Fukuma, T.; Takahashi, Y. Nanoscale reactivity mapping of a single-crystal boron-doped diamond particle. *Anal. Chem.* **2021**, *93* (14), 5831−5838.
(81) Ivandini, T. A.; Watanabe, T.; Matsui, T.; Ootani, Y.; Iizuka, S.; Toyoshima, R.; Kodama, H.; Kondoh, H.; Tateyama, Y.; Einaga, Y. Influence of surface orientation on the electrochemical properties of boron-doped diamond. *J. Phys. Chem. C* **2019**, *123* (9), 5336−5344.
(82) Michaelson, H. B. The work function of the elements and its periodicity. *J. Appl. Phys.* **1977**, *48* (11), 4729−4733.
(83) Sze, S. M.; Li, Y.; Ng, K. N. *Physics of Semiconductor Devices*, 4th ed.; Wiley, 2021.
(84) Li, S. S. *Semiconductor Physical Electronics*, 2nd ed.; Springer, 2006.
(85) Gomes, W. P.; Vanmaekelbergh, D. Impedance spectroscopy at semiconductor electrodes: Review and recent developments. *Electrochim. Acta* **1996**, *41* (7−8), 967−973.

https://doi.org/10.1021/jacsau.4c00006
JACS Au 2024, 4, 1184−1193